DESIGN AND TESTING OF HYDRAULIC DRIVE SYSTEM FOR CRAWLER-TYPE TIGER-NUT HARVESTER

/

履带式油莎豆收获机液压驱动行走系统的设计与试验

Zhe QU, Jianhao ZHANG, Jintao LE, Xilong WANG, Haihao SHAO, Huihui ZHAO, Zhijun LV, Wanzhang WANG* [1]
College of Mechanical and Electrical Engineering, Henan Agricultural University, Zhengzhou 450002, China
Tel: 17513301867; E-mail: quzhe071171@henau.edu.cn
Corresponding author: Wanzhang Wang
DOI: https://doi.org/10.35633/inmateh-76-17

Keywords: *tiger-nut harvester, crawler, hydraulic drive, field trial*

ABSTRACT

Tiger-nut is widely cultivated in sandy soils across China, and the mechanization level for harvesting remains low. Harvesters are mainly medium- and small-sized tractor-drawn models, which exhibit weak driving capability, a large turning radius, and poor stability. This paper presents the design of a crawler-type tiger-nut harvester hydraulic-driven travel system, with the required hydraulic motor displacement of 44.65 mL·r^{-1} and hydraulic pump displacement of 44.58 mL·r^{-1}. Experimental results from the harvester showed that the harvester's linear travel deviation rate ranged from 1.19% to 2.10%, with an average travel speed of 1.08 m·s^{-1} and the average value of radius for forward left turn and forward right turn is 2740 mm and 2748 mm. The harvester can achieve bidirectional stepless speed regulation in the field, ensuring stable harvesting performance and meeting the design requirements for the tiger-nut harvester.

摘要

油莎豆多种植于中国的沙土地，目前油莎豆机械化收获水平低，现有收获机以中小型牵引式为主，存在驱动能力弱、转弯半径大和行驶稳定性差等问题。本文设计了一种履带式油莎豆收获机液压驱动行走系统，计算得出所需的液压马达排量为 44.65 mL·r^{-1}，液压泵排量为 44.58 mL·r^{-1}。样机试验结果表明：收获机直线行走偏移率为 1.19%-2.10%，平均行走速度为 1.08 m·s^{-1}，前进左转和前进右转的半径平均值分别为 2740 mm 和 2748 mm。收获机在田间能够实现双向无级调速，收获作业性能稳定，满足油莎豆收获机设计要求。

INTRODUCTION

Tiger-nut, often referred to as the "king of oilseed crops," contains rich nutrients in its underground tubers, which can be used to extract edible oil, sugars, and produce beverages, offering significant economic value *(Roselló-Soto et al., 2018; Edo et al., 2024; Wang et al., 2021; Cantalejo et al., 1997)*. China currently relies on imports for more than 70% of its oilseed crops. In the context of the current international situation, the development of the tiger-nut industry holds great strategic importance in addressing Chinese edible oil security issues *(Zhang et al., 2020; Zhang et al., 2024)*.

Mechanized harvesting is a critical and challenging phase in the full mechanization process of tiger-nut production. To optimize harvesting, tiger-nut is best cultivated in sandy soils. Tiger-nut harvesters are generally classified into two types based on their travel mechanism: towed and self-propelled *(Shang et al., 2004)*. In foreign countries, tiger-nut harvesters are typically towed by high-horsepower tractors to perform digging and transportation tasks. However, these harvesters have large structures with limited functions and require coordination with transport vehicles for synchronized harvesting, making them unsuitable for small-scale farms. Currently, the majority of tiger-nut harvesters in China are small- and medium-sized towed models, which suffer from issues such as weak driving power, large turning radius, and poor stability. These shortcomings negatively impact the digging, cleaning, and screening quality, severely limiting the development of the tiger-nut industry *(Xu et al., 2016; Wei et al., 2023)*.

[1] *Zhe Qu, Associate Professor. Ph.D. Eng.; Jianhao Zhang, M.S. Stud. Eng.; Jintao Le, M.S. Stud. Eng.; Xilong Wang, M.S. Stud. Eng.; Haihao Shao, M.S. Stud. Eng.; Huihui Zhao, Lecturer. Ph.D. Eng.; Zhijun Lv, Lecturer. Ph.D. Eng.; Wanzhang Wang, Professor. Ph.D. Eng.*

The tracked travel system provides low ground pressure, high adhesion, strong load-bearing capacity, and a small turning radius *(Jun et al., 2013; McBride et al., 2000; Leggieri et al., 2022)*. The hydraulic drive system enables stepless speed regulation, offering smooth transmission, ease of operation, and rapid response *(Lv et al., 2024; Guo et al., 2025; Zhao et al., 2025)*. By combining the advantages of both systems, a smooth and efficient harvest of tiger-nut can be achieved. Therefore, this paper presents the design of a crawler-type self-propelled tiger-nut harvester with a hydraulic drive system, to enhance the harvester's adaptability and ensure the stability of the harvesting operation.

MATERIALS AND METHODS

Structure and technical parameters of the machine

The developed tiger-nut harvester comprises an excavating device, cab, lifting device, engine, material box, feeding device, screening device, drive system, crawler travel device, and other components. The overall structure of the machine is shown in Fig. 1, and the main parameters are shown in Table 1.

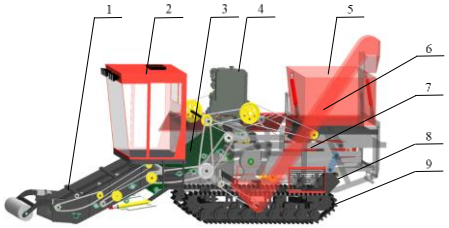

Fig. 1 - The whole structure of tiger-nut harvester

1. Excavating device; 2. Cab; 3. Lifting device; 4. Engine; 5. Material box; 6. Feeding device; 7. Screening device; 8. Drive system; 9. Crawler travel device

Table 1

The main technical parameters of tiger-nut harvester

Parameters	Values
Unladen mass [kg]	7500
Full load mass [kg]	10000
Overall dimensions [mm]	6800×2500×3200
Rated engine power [kW]	103
Rated engine speed [r·min^{-1}]	2300
Working width [mm]	1800
Harvesting speed [m·s^{-1}]	0-0.3
Travel speed [m·s^{-1}]	0-1

The general structure of the hydraulic drive system

The key components of the hydraulic drive system designed in this paper include a hydraulic stepless speed changer, reducer, direction cylinder, and other elements, as shown in Fig. 2.

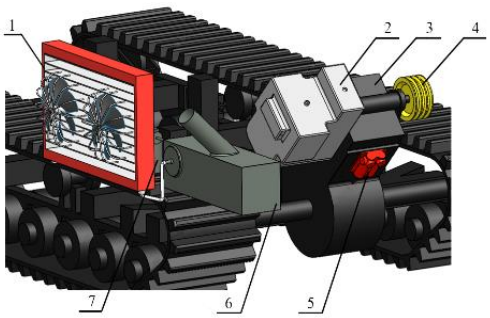

Fig. 2 - The overall structure of the hydraulic drive system

1. Radiator; 2. Stepless speed changer; 3. Reducer; 4. Power input; 5. Direction cylinder; 6. Hydraulic oil tank; 7. Filter

The basic parameters of the hydraulic drive system are shown in Table 2.

Table 2

Basic parameters of hydraulic drive system

Parameters	Values
Transmission mode	stepless gearbox
Steering type	unilateral brake steering
Pump power input method	a leather drive belt
Hydraulic pump displacement [mL·r^{-1}]	46
Maximum system pressure [MPa]	32
Rated system pressure [MPa]	16
Hydraulic motor displacement [mL·r^{-1}]	46
Hydraulic pump input speed [r·min^{-1}]	2300
Low speed reduction ratio	90
High speed reduction ratio	30

Working principle of hydraulic drive system

The working principle of the hydraulic drive system designed in this paper is illustrated in Fig. 3.

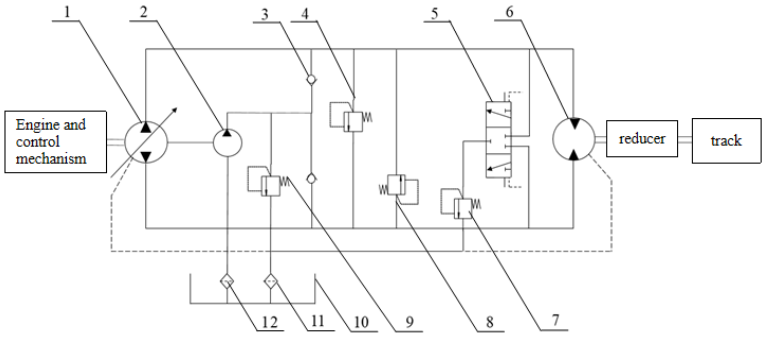

Fig. 3 - Hydraulic schematic of the drive and travel system

1. Variable pump; 2. Charge pump; 3. Check valve; 4. High pressure relief valve; 5. Flush valve; 6. Hydraulic motor; 7. Low pressure relief valve; 8. High pressure relief valve; 9. Charge relief valve; 10. Hydraulic oil tank; 11. Oil return filter; 12. Oil suction filter

The hydraulic pump in the hydraulic drive system is a bidirectional piston variable displacement pump, while the charge pump is a gear pump. The hydraulic pump is connected directly to the power input shaft, supplying hydraulic fluid to the system. The hydraulic motor is a bidirectional piston fixed displacement motor, with its output connected to a reducer, converting hydraulic energy into mechanical output. The charge pump, charge relief valve, and other components form the charge circuit, which replenishes hydraulic fluid in the system and maintains stable system pressure. The flush valve, low pressure relief valve, and oil return filter form the flushing circuit, which aids in reducing system temperature and ensuring proper lubrication. The check valve and high pressure relief valve together make up the protection circuit, maintaining stable system pressure. The system operates as follows: The engine drives the hydraulic pump via a belt, powering the hydraulic system. The hydraulic pump draws fluid from the oil tank, converting the engine's mechanical energy into hydraulic energy. As the oil flows through the circuit, it drives the hydraulic motor, which generates rotational speed and torque, converting hydraulic energy back into mechanical energy. Once the hydraulic motor discharges the oil, the oil flows directly into the intake of the hydraulic pump, starting the next cycle. If the system experiences low pressure or oil leakage, the charge circuit replenishes the oil. To adjust speed or reverse the motion, the operator uses the control handle to adjust the servo control valve. This action moves the servo cylinder, which adjusts the tilt angle of the hydraulic pump's swashplate, changing the pump's displacement and flow rate, enabling continuous variable speed control. When the system is idle, the hydraulic fluid returns to the oil tank through the flushing circuit.

Design of key components of hydraulic drive system

- **Traction Performance Analysis and Calculations**

The traction performance of a travel system is the traction work capacity exerted under specified ground conditions and its efficiency. The force model of the harvester while traveling is shown in Fig. 4.

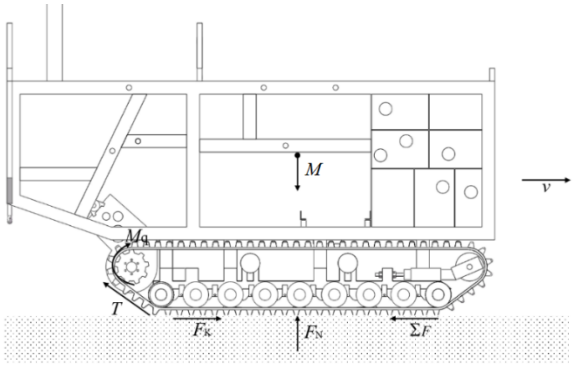

Fig. 4 - Force model of the tracked travel device during operation

From the mechanical model, it can be seen that under the action of the driving moment M_q, the track generates a tension T with the value:

$$T = \frac{M_q}{r_q} = \frac{i_1 \cdot \varphi_e \cdot M_e}{r_q} \quad (1)$$

where:

φ_e is the engine-to-drive-wheel mechanical efficiency, 0.95;

M_q is the drive-wheel torque, [N·m];

r_g is the drive-wheel radius of 0.16 [m] *(Han et al., 2023)*;

Neglecting the friction loss of tension T, the track attachment force F_k is equal to the track tension. The normal operation of the tiger-nut harvester in the field requires overcoming the rolling resistance F_p from the ground, the inertial resistance of the system F_i, the internal resistance of the system F_f, and the ramp resistance F_z and the digging resistance F_c when traveling on a ramp. Rolling resistance is mainly the normal and tangential forces generated by contact with the ground and the deformation of the tracks and the ground under full gravity, which is related to the resistance coefficient and the weight of the whole machine. The main working environment of the tiger-nut harvester is sandy loam soil, and the rolling resistance coefficient is taken as 0.15 *(Pan et al., 2014)*.

$$M = mg \quad (2)$$

$$F_p = f\ M\ \cos\alpha \quad (3)$$

where:

M is the gravity of the harvester, [N];

m is the mass of the harvester when fully loaded, [kg], calculated as 10000 kg;

α is the slope of the ramp, taken as 20°;

g is the acceleration of gravity, [m·s^{-2}];

f is the rolling resistance coefficient;

The rolling resistance F_p = 14095.39 N was calculated.

Inertial resistance is calculated by the following formula:

$$F_i = \frac{2Mv}{gt} \quad (4)$$

where:

v is the travel speed during operation, taken as 0.4 [m·s^{-1}];

t is the acceleration time, taken as 3 s;

The inertial resistance F_i = 2666.67 N was calculated.

The internal resistance of the system is related to the overall lubrication and precision and is calculated from the mass of the whole machine and the internal resistance coefficient:

$$F_f = \partial M \tag{5}$$

where:

∂ is the internal friction drag coefficient, typically 0.05-0.07 *(Ji et al., 2013)*, taken as 0.07;

The internal resistance F_f= 7000 N was calculated.

When the harvester travels uphill or downhill, the component of gravitational force acting along the slope direction generates resistance. This resistance is related to the slope and is calculated using the following formula:

$$F_z = M \sin\alpha \tag{6}$$

The ramp resistance F_z = 34202.01 N was calculated.

When the tiger-nut harvester operates in the field, the travel system is simultaneously subjected to digging resistance. The maximum digging depth of the harvester's digging mechanism is 200 mm, and the digging width corresponds to the full working width of 1800 mm (*Lv et al., 2022; Zhang et al., 2021*). The digging resistance F_c is calculated as follows:

$$F_c = 2\tau h_c W \tag{7}$$

where: τ is the coefficient of integration per unit of transverse area of the soil mound *(Han et al., 2023)*, taken as 5 N·cm^{-2};

h_c is the depth of excavation, [mm];

W is the width of excavation, [mm];

The excavation resistance F_c = 36000 N was calculated.

The maximum traction required by the system is equal to the sum of all resistance forces:

$$F_q = F_p + F_i + F_f + F_z + F_c \tag{8}$$

where:

F_q is the total tractive force, [N];

The total tractive force F_q = 93964.07 N was calculated.

The ground adhesion F_φ was calculated by the following equation:

$$F_\varphi = \varphi M \tag{9}$$

where: φ is the adhesion coefficient factor taken as 1.0 *(Liu et al., 2022)*;

The ground adhesion F_φ = 100000 N was calculated.

A comparative analysis of the calculated data shows that the total traction force F_q is smaller than the ground adhesion force F_φ, indicating that the system meets the calibration requirements and the harvester will not experience slippage during field operation.

The drive wheel speed and driving torque are calculated according to the following formula:

$$n_q = \frac{60v}{2\pi r_q} \times 10^3 \tag{10}$$

$$M_q = \frac{1}{2} \sum F \cdot r_q \times 10^{-3} \tag{11}$$

where:

n_q - maximum speed of the drive wheel, [r·min^{-1}];

r_q - radius of the drive wheel, 160 [mm];

M_q - driving torque, [N·m];

The drive wheel speed n_q = 24 r·min^{-1} and the drive torque M_q = 8000 N·m were calculated.

- **Determination of travel system operating pressure**

The operating environment of the crawler-type tiger-nut harvester consists of sandy loam. The hydraulic system's working pressure is initially set at 14 MPa, with a maximum pressure of 32 MPa *(Dong et al., 2005)*.

- **Parameterization of hydraulic motors**

The hydraulic motor output speed n_m, torque M_m and displacement V_m are as follows.

$$n_m = n_q \cdot i_1 \tag{12}$$

$$M_m = \frac{M_q}{i_1 \cdot \eta_1 \cdot \eta_2} \tag{13}$$

$$V_m = \frac{2\pi M_m}{\Delta P \cdot \eta_3} \tag{14}$$

The synthesized equation yields:

$$V_m = \frac{\pi F_q r_q}{\Delta P \cdot \eta_1 \cdot \eta_2 \cdot \eta_3 \cdot i_1} \tag{15}$$

where:

i_1 is the low-speed reduction ratio (field operation reduction ratio), 90;

η_1 is the hydraulic motor mechanical efficiency, taken as 0.95;

η_2 is the reduction gearbox mechanical efficiency, taken as 0.99;

η_3 is the hydraulic motor volumetric efficiency, taken as 0.95;

ΔP is the system pressure, MPa;

Bringing in the data, it was calculated that the motor speed m_n = 2160 r·min^{-1}, the torque applied to the motor M_m = 94.51 N·m, and the motor displacement V_m = 44.65 mL·r^{-1} during the stable operation of the harvester in the field.

- **Calculation of hydraulic pump parameters**

In the selected hydrostatic (HST) transmission system, the hydraulic pump and hydraulic motor are connected in an integrated closed-loop configuration. By ignoring system flow losses and using the motor displacement along with the desired operating speed, the system flow rate can be calculated. This flow rate is then used to determine the required displacement of the hydraulic pump V_p:

$$Q_m = \frac{n_m \cdot V_m}{1000\eta_3} \tag{16}$$

$$Q_p = Q_m \tag{17}$$

$$V_p = \frac{1000Q_p}{\eta_p \cdot \eta_4} \tag{18}$$

Available:

$$V_p = \frac{n_m \cdot V_m}{\eta_p \cdot \eta_3 \cdot \eta_4} \tag{19}$$

where:

Q_p is the hydraulic pump flow rate, [L·min^{-1}];

n_p is the pump power input speed, [r·min^{-1}];

η_4 is the hydraulic pump volumetric efficiency, 0.99;

The hydraulic pump output flow rate Q_p = 101.52 L·min^{-1} and the hydraulic pump displacement V_p = 44.58 mL·r^{-1} were calculated.

The displacement of the charge pump is 20-25% of the displacement of the variable pump, and the charge pressure is less than 3 MPa.

$$V_p' = (0.2 \sim 0.25) V_p \tag{20}$$

The charge pump displacement V'_p was calculated to be 8.92-11.15 mL·r^{-1} based on the data.

- **Other hydraulic components**

When designing and selecting tubing, fittings, and hydraulic fluid, the process should adhere to relevant national standards *(Standardization Administration of the People's Republic of China, 2021; Standardization Administration of the People's Republic of China, 2022)*, while considering factors such as connection reliability, sealing performance, pressure loss, and overall cost.

The inner diameter of the fuel line is calculated as follows:

$$d = \sqrt{\frac{4q}{\pi v_0}} \times 10^3 \quad (21)$$

where: d is the diameter of the hydraulic pipe, [mm];

q is the flow rate of the hydraulic fluid, [$m^3 \cdot s^{-1}$];

v_0 is the flow rate of the hydraulic fluid, taken as 4 $m \cdot s^{-1}$;

The calculated inner diameter was d = 18.3 mm. According to standard requirements, the hose inner diameter was specified as 20 mm, and appropriate tube fittings were selected accordingly.

- **Selection of hydraulic drives**

Based on the hydraulic principles and component parameters used in the design calculations, a Heckert HT series variable pump with a displacement of 46 $mL \cdot r^{-1}$ and a rated pressure of 16 MPa was selected, along with an integrated hydraulic drive unit consisting of a hydraulic pump and motor. The configuration is shown in Figure 5, and the corresponding parameters are listed in Table 3.

Fig. 5 - Hydraulic drive device

Table 3

Hydraulic drive device parameters

Parameters	Values
System displacement [$mL \cdot r^{-1}$]	46
Charge pump displacement [$mL \cdot r^{-1}$]	10
Rated pressure [bar]	160
Maximum pressure [bar]	320
Control system	mechanical servo
Maximum speed [$r \cdot min^{-1}$]	3300

RESULTS

Performance Tests

- **Site testing**

The field tests focused on evaluating the harvester's straight-line travel performance, response characteristics, and parking brake effectiveness on slopes, as well as measuring its maximum travel speed and operational stability.

- **Travel straightness test**

The straight-line movement test of the harvester is conducted according to the GB/T 15370.4-2012 standard *(Standardization Administration of the People's Republic of China, 2012)*. A 20 m correction zone and a 30 m test zone are defined within the test field. The test factors include the hydraulic pump displacement (maximum and intermediate displacements) and load size (no load, 200 kg load, and 500 kg load). The deviation rate is used as the performance indicator to assess the straightness of the movement process.

The travel offset rate was calculated based on the formula:

$$\Delta C = X_1 - X_2 \quad (22)$$

$$H = \frac{|\Delta C|}{S} \quad (23)$$

where: X_1 is the perpendicular distance between the track and the reference straight line before the test, [m];

X_2 is the perpendicular distance between the track and the reference straight line after the test, [m];

H is the offset rate, [%]; ΔC is the offset, [m]; S is the test distance, [m].

The results of the offset rates obtained for different operating conditions are shown in Table 4.

Table 4

Offset test results

Hydraulic pump displacement	Number of tests	Unladen	200 kg Load	500 kg Load
		Offset rate [%]	Offset rate [%]	Offset rate [%]
Maximum displacement	1	0.14	0.15	0.12
	2	0.09	0.12	0.19
	3	0.15	0.20	0.11
Intermediate displacement	1	0.10	0.15	0.12
	2	0.18	0.13	0.16
	3	0.16	0.12	0.14

The field test results show that the deviation rate of the harvester ranges from 0.09% to 0.20%, significantly lower than the standard requirement of 6%, demonstrating that the harvester exhibits excellent straight-line movement and that the hydraulic drive system fulfills the performance criteria. Additionally, the deviation rate remains relatively consistent across different displacements, indicating that the displacement of the hydraulic pump has a minimal effect on the straight-line movement performance. Furthermore, the deviation rate remains relatively consistent under different loads, suggesting that the hydraulic drive system demonstrates robust adaptability to different load conditions.

- **Travel speed measurement test**

The travel speed measurement test is conducted to verify the speed control stability of the designed hydraulic drive system and to determine the maximum field travel speed. The theoretical maximum travel speed of the designed harvester is calculated using the following formula:

$$n_{qm} = \frac{n_m}{i_2} \tag{24}$$

$$v_m = \frac{2\pi r_q \cdot n_{qm}}{60} \tag{25}$$

where: n_{qm} is the theoretical travel speed of the driving wheel, [r·min^{-1}];

n_m is the output speed of the hydraulic motor, [r·min^{-1}];

i_2 is the high speed reduction ratio, 30;

v_m is the maximum theoretical travel speed, [m·s^{-1}];

The maximum theoretical travel speed of the crawler-type tiger-nut harvester was calculated to be 1.18m·s^{-1}.

In the test field, a 50-meter distance was measured as the travel speed measurement interval. Buffer zones for acceleration and deceleration were marked 10 meters before and after the measurement interval. The central 30-meter section was divided into six equal intervals, each 5 meters in length. The time to traverse each 5-meter interval was recorded, and the speed for each interval, as well as the average speed over the entire section. The harvester was tested in an unloaded state under high gear conditions, with the control lever for speed pushed to its maximum, and the test was repeated three times. The 18 speed measurements obtained from the six segments across the three tests were processed as shown in Fig. 6.

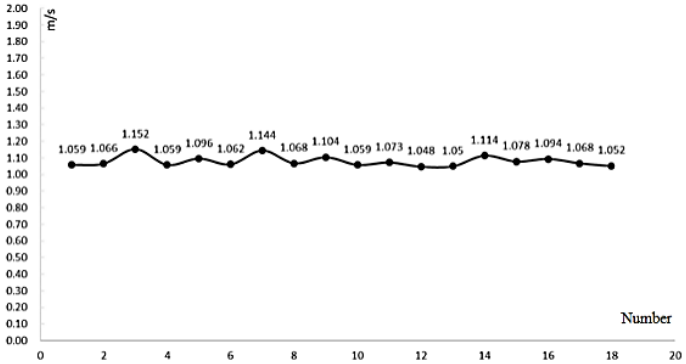

Fig. 6 - Speed stability analysis

As shown in Figure 6, the measured field travel speed ranged from 1.05 to 1.15 m·s^{-1}, with an average speed of 1.08 m·s^{-1} and a standard deviation of 0.03 m·s^{-1}. The overall data exhibited minimal fluctuation, with no significant outliers, indicating good speed stability of the hydraulic drive system. However, due to internal leakage within hydraulic components, track slippage, and other influencing factors, the maximum measured travel speed was slightly lower than the theoretical value of 1.18 m·s^{-1}. Nonetheless, the maximum travel speed of the harvester meets the design requirements, and the travel process remains stable and reliable.

- **Starting and braking performance tests**

The time required for the harvester to accelerate from rest to maximum speed is defined as the startup acceleration time, which reflects the responsiveness of the hydraulic drive system. The time for the harvester to decelerate from maximum speed to a complete stop is termed the braking deceleration time. Three measurements were conducted, and the average value was taken. The average values are shown in Table 5.

The relationship between the drive wheel speed monitored by the tachometer and the travel speed is described by the following equation:

$$n_q = \frac{60}{2\pi r_q} v \tag{26}$$

As can be seen from the speed test results in Fig. 6, the maximum travel speed obtained in the field test was 1.15 m·s^{-1}, which was substituted into the data to calculate the driving wheel speed at the maximum speed of 64.46 r·min^{-1}.

Table 5

Starting and braking performance measurement results

Ordinal number	Start-up acceleration time [s]	Brake deceleration time [s]
1	3.1	1.5
2	3.7	0.8
3	3.3	1.2
Average value	3.4	1.2

As shown in Table 5, the hydraulic drive system of the harvester demonstrates good startup and braking performance. The startup time is close to the simulation response time of 2.8 seconds, which also validates the accuracy of the simulation. The higher measured response time compared to the simulation may be due to the manual stopwatch measurement, which could introduce errors in reaction time.

- **Ramp parking brake test**

The ramp parking brake performance test was conducted in accordance with GB/T 3871.6-2006 *(Standardization Administration of the People's Republic of China, 2006)*. The harvester was driven steadily onto a ramp, and the engine was then shut off to perform parking brake tests in both uphill and downhill conditions. Each test maintained a parking duration of 3 minutes. The test setup is illustrated in Figure 7.

Fig. 7 - Ramp braking test

a. Uphill parking brake test *b. Downhill parking brake test*

The test results showed that the harvester remained stationary during the entire ramp parking duration, demonstrating excellent parking stability. This meets the test requirements and indicates that the hydraulic system provides reliable parking brake performance on slopes.

Field trials

To comprehensively evaluate the performance of the harvester and its hydraulic drive system, field tests on straight-line driving and turning performance were conducted after the simulations and field trials of the hydraulic system.

- **Linear travel test**

In a test field, the harvester was driven at maximum speed without adjusting the control handle to further assess the straight-line driving performance of the designed drive system. Three sets of tests were conducted, and the track marks were processed to evaluate the straight-line performance. The results are shown in Fig.8.

a. First test track processing

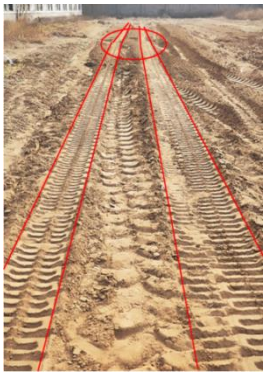

b. Second test track processing

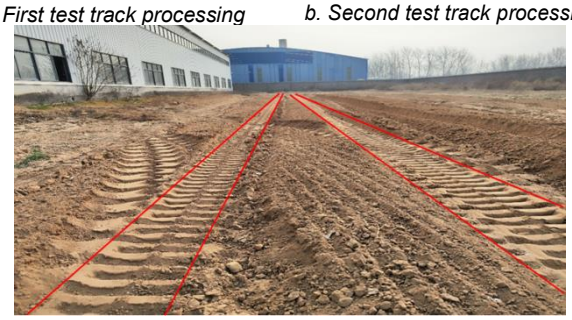

c. Third test track processing

Fig. 8 - Field straight-line travel test

According to the field straight-line driving performance test, the harvester's deviation rate ranges from 1.19% to 2.10%. The sideways slipping of the harvester, caused by soft soil and subsidence, leads to a slightly higher deviation rate compared to the field test, but it still meets the national standard requirements. The test results indicate that the harvester has good straight-line driving performance, meeting the requirements for tiger-nut harvesting.

- **Field steering trials**

In order to verify the steering ability and steering radius of the harvester in the field, three tests were conducted with forward left and right turns respectively, and the steering test and radius measurement process are shown in Fig. 9, and the results are shown in Table 6.

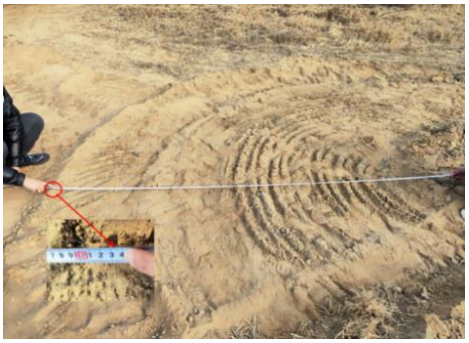

Fig. 9 - Field turning test

Table 6

Field Turning Test Results

Serial number	Left Turning Radius [mm]	Right Turning Radius [mm]
1	2714	2807
2	2763	2726
3	2742	2711
Average value	2740	2748

The theoretical radius R_t is 2720 mm when steering in the field, and the average value of radius for forward left turn and forward right turn is 2740 mm and 2748 mm. There is a track offset within the permissible range when steering, and it can be accomplished by unilateral braking steering in the field as required.

CONCLUSIONS

(1) To improve the adaptability of the tiger-nut harvester and ensure stable harvesting operation, a hydraulic drive system for the crawler-type harvester was designed. The required displacement of the hydraulic motor was calculated to be 44.65 mL·r^{-1}, and the displacement of the hydraulic pump was determined to be 44.58 mL·r^{-1}. A unified hydrostatic drive unit with a displacement of 46 mL·r^{-1} and a system pressure of 16 MPa was selected.

(2) Field evaluations demonstrated that the harvester exhibits a straight-line deviation rate of 1.19–2.10% and an average travel speed of 1.08 m·s^{-1}. The effective implementation of the steering mechanism, which reliably regulates turning performance under various field conditions, confirms the system's capacity to achieve stable and efficient harvesting operations.

(3) Field trials in sandy loam soils show that the hydraulic drive system performs stably under varying loads and speeds, with low deviation and precise turning. These results confirm its reliability for tiger-nut harvesting and support further optimization and industrial application.

ACKNOWLEDGEMENTS

This research was supported by the Key R&D and Demonstration Program of Henan Province (Science and Technology Breakthrough) (Grant Nos. 252102110351 and 242102110378) and the National Key R&D Program of China (Grant No. 2019YFD1002602).

REFERENCES

[1] Cantalejo, J. M. (1997). Analysis of volatile components derived from raw and roasted earth-almond (cyperus esculentus L.). *Journal of Agricultural & Food Chemistry*, Vol.45, No.5, pp.1853-1860. Heidelberg/Germany.

[2] Dong, W. L. (2005). *Hydraulic design handbook*. China Machine Press, Beijing/China.

[3] Edo, G. I., Samuel, P. O., Nwachukwu, S. C., Ikpekoro, V. O., Promise, O., Oghenegueke, O., Ongulu, J., Otunuya, C. F., Rapheal, O. A., Ajokpaoghene, M. O., Okolie, M. C., & Ajakaye, R.S. (2024). A review on the biological and bioactive components of Cyperus esculentus L.: Insight on food, health and nutrition. *Journal of the Science of Food and Agriculture*, Vol.104, No.14, pp.8414–8429. UK.

[4] Guo, T., Zhang, D., Lin, S., Zhang, T., & Lu, M. (2025). Research on hydraulic drive chassis of tobacco harvester in southern hilly area. *INMATEH - Agricultural Engineering*, Vol.75, No.1, pp.819–830. DOI: https://doi.org/10.35633/inmateh-75-70

[5] Han, M. H. (2023). *Design and experiment of traveling device and hydraulic drive system for tiger-nut harvester (油莎豆收获机履带行走装置及其液压驱动系统的设计与试验)*. Master's dissertation, Henan Agricultural University, Zhengzhou/China.

[6] Ji, L. X. (2013). *Design and performance study of the rubber crawler combined with high-range sprayer. Master's dissertation (橡胶履带式喷雾机行走装置的设计及性能研究)*, Nanjing Forestry University, Nanjing/China.

[7] Jun, H.-J., Kang, T.-G., Lee, C.-S., Lee, C.-K., Choi, D.-K., & Choi, C. (2013). Development of a crawler type vehicle to travel in water paddy rice field for water-dropwort harvest. *Journal of Biosystems Engineering*, Vol.38, No.4, pp.240–247. Korea.

[8] Leggieri, S., Canali, C., & Caldwell, D. G. (2022). Design of the crawler units: Toward the development of a novel hybrid platform for infrastructure inspection. *Applied Sciences*, Vol.12, No.11, Article 5579. Switzerland.

[9] Liu, F. S. (2022). *Chassis optimization of crawler self-propelled potato harvester (履带自走式马铃薯收获机的底盘优化)*. Master's dissertation, Huazhong Agricultural University, Wuhan/China.

[10] Lv, X. R., Fu, Y., Cheng, X. P., Zhang, F. G., Len, Y. C., Han, D. D. (2024). Design and performance test of remote driving control system of small agricultural hydraulic chassis. *INMATEH – Agricultural Engineering*, Vol.72, No.1, pp.255–264. DOI: https://doi.org/10.35633/inmateh-72-24

[11] Lv, Y. L. (2022). *Design and experiment of excavating and hoisting device of cyperus esculentus harvester (油莎豆收获机挖掘升运装置设计与试验).* Master's dissertation, *Henan Agricultural University*, Zhengzhou/China.
[12] McBride, R. A., McLaughlin, N. B., & Veenhof, D. W. (2000). Performance of wheel and track running gear on liquid manure spreaders. *Canadian Agricultural Engineering*, Vol.42, No.1, pp.19–25. Canada.
[13] Pan, D. J. (2014). *The design of self-propelled machine integrating the function of fertilization and plant protection for growing grape and Chinese wolfberry (自走式枸杞葡萄施肥植保一体机的设计)*. Master's dissertation, Ningxia University, Yinchuan/China.
[14] Roselló-Soto, E., Poojary, M. M., Barba, F. J., Lorenzo, J. M., Manes, J., & Moltó, J. C. (2018). Tiger nut and its by-products valorization: From extraction of oil and valuable compounds to development of new healthy products. *Innovative Food Science and Emerging Technologies*, Vol.45, pp.306–312. Netherlands.
[15] Shang, S. Q., Wang, F. Y., Liu, S. G., Zhao, Z. H., & Wang, J. C. (2004). Research situation and development trend on peanut harvesting machinery (花生收获机械的研究现状与发展趋势). *Transactions of the CSAE*, Vol.20, No.1, pp.20–25. Shenyang/China.
[16] Standardization Administration of the People's Republic of China. (2006). *Agricultural tractors—Test procedures—Part 6: Determination of braking performance*. Beijing/China.
[17] Standardization Administration of the People's Republic of China. (2012). *General requirement of agricultural tractors—Part 4: Crawler tractors*. Beijing/China.
[18] Standardization Administration of the People's Republic of China. (2021). *Fluid power systems and components—Outside diameters of tubes and inside diameters of hoses*. Beijing/China.
[19] Standardization Administration of the People's Republic of China. (2022). *Rubber hoses and hose assemblies—Rubber-covered spiral-wire-reinforced hydraulic types for oil-based or water-based fluids*. Beijing/China.
[20] Wang, L., Hu, C., Guo, W. S., He, X. W., Wang, X. F., & Jian, J. M., et al. (2021). The effects of moisture content and loading orientation on some physical and mechanical properties of tiger nut. *American Journal of Biochemistry and Biotechnology*, Vol.17, No.1, pp.109–117. Ghana/Africa.
[21] Wei, Z. C., Wang, X. H., Li, X. Q., Wang, F. M., Li, Z. H., & Jin, C. Q. (2023). Design and experiment of crawler self-propelled sorting type potato harvester (履带自走式分拣型马铃薯收获机设计与试验). *Transactions of the Chinese Society for Agricultural Machinery*, Vol.54, No.2, pp.95–106. Zibo/China.
[22] Xu, Y. J. (2016). Design and research of a new type of cyperus esculentus harvesting machine (新型油莎豆收获机的设计与研究). Master's dissertation, *China Agricultural University*, Beijing/China.
[23] Zhang, H. M., Zhou, Z., Lv, Z. J., Wang, W. Z., He, H., & Lv, Y. L. (2021). Kinematic analysis and testing of vibratory sieving mechanism for cyperus esculentus L. harvester (油莎豆收获筛分机构运动学分析与试验). *Journal of Chinese Agricultural Mechanization*, Vol.42, No.10, pp.92–99. Zhengzhou/China.
[24] Zhang, X. M., & Dong, X. R. (2020). The impact of Sino-US trade war on China's soybean market (中美贸易战对我国大豆市场的影响). *Modern Business Trade Industry*, Vol.41, No.14, pp.19–20. Bengbu/China.
[25] Zhang, Z., Jiang, H., He, X., Zhang, F., Wang, J., & Wang, D. (2024). Design and test of threshing and cleaning device for Cyperus esculentus L. combine harvester. *INMATEH - Agricultural Engineering*, Vol.72, No.1, pp.798–808. DOI: https://doi.org/10.35633/inmateh-72-71
[26] Zhao, Y., Liu, W., Song, S., Liu, P., Wang, Y., & Zhang, G. (2025). Design of the leveling system for the wheeled adaptive chassis in hilly and mountainous areas. *INMATEH - Agricultural Engineering*, Vol.75, No.1, pp.253–268. DOI: https://doi.org/10.35633/inmateh-75-22